Int. J. Heat Mass Transfer. Vol. 21, pp. 1555–1564
Pergamon Press Ltd. 1978. Printed in Great Britain

THERMAL CONVECTION IN ROTATING SPHERICAL ANNULI—2. STRATIFIED FLOWS

R. W. DOUGLASS
Department of Mechanical Engineering, University of Nebraska,
Lincoln, NE 68588, U.S.A.

B. R. MUNSON
Department of Engineering Science and Mechanics and Engineering Research Institute,
Iowa State University, Ames, IA 50011, U.S.A.

and

E. J. SHAUGHNESSY
Department of Mechanical Engineering and Materials Science,
Duke University, Durham, NC 27705, U.S.A.

(*Received* 17 *June* 1977 *and in revised form* 9 *March* 1978)

Abstract—The steady combined thermal convection of a viscous Boussinesq fluid contained between two concentric spheres is considered. The spheres are maintained at different temperatures and rotate about a common axis with different angular velocities. A uniform radial gravitational field acts on the fluid. Approximate solutions to the governing equations are obtained with a modified Galerkin technique for moderate Reynolds numbers. The resulting flow patterns, temperature distributions, and heat-transfer and torque characteristics are presented for several angular velocity ratios and degrees of stratification. It is shown that increasing the buoyancy forces alters the primary and secondary flow patterns as well as the temperature distributions. The total rate of heat transfer and torque are subsequently enhanced.

NOMENCLATURE

c, specific heat;
$\mathbf{e}_r$, radial unit vector;
g_0, gravitational acceleration constant;
Gr, Grashof number $= g_0\beta(T_2 - T_1)R_2^3/\nu^2$;
Pr, Prandtl number $= \mu c/\kappa$;
$q(\theta)$, local wall heat-transfer rate;
Q, total heat-transfer rate;
r, radial coordinate;
R_1, R_2, inner and outer radius of the spheres;
Ra, Rayleigh number $= GrPr$;
Re, Reynolds number $= \omega_0 R_2^2/\nu$;
$T(r,\theta)$, fluid temperature;
T_1, T_2, inner and outer surface temperatures;
v, velocity component.

Greek symbols

β, coefficient of volume expansion of the fluid;
$\zeta(r,\theta)$, dimensionless temperature function;
η, radius ratio $= R_1/R_2$;
θ, latitudinal coordinate;
κ, thermal conductivity;
μ, viscosity of the fluid;
$\tilde{\mu}$, angular velocity ratio $= \omega_2/\omega_1$;
ν, kinematic viscosity.
π, 3.1415---;
ϕ, longitudinal coordinate;
$\psi(r,\theta)$, stream function;
$\omega(r,\theta)$, angular velocity of the fluid;
ω_1, ω_2, angular velocity of the inner and outer spheres;
ω_0, reference angular velocity;
$\Omega(r,\theta)$, angular momentum function.

Subscripts

c, conduction;
r,θ,ϕ, vector components.

Superscripts

$\hat{}$, physical variable.

1. INTRODUCTION

WE CONSIDER in this second part the steady thermal convection of a viscous Boussinesq fluid contained between two concentric spheres. The spheres are maintained at constant, prescribed temperatures and angular velocities. Each sphere rotates about a common axis. The gravitational force is assumed to be uniform in the radial direction. We consider flows exhibiting both natural and forced convection phenomena. As stated in Part 1, the general problem approximates several geophysical flows and is also a comparatively simple example of the effects of rotation on thermal convection. The interaction of buoyancy forces with the secondary flow arising from the differential rotation produces many interesting convective phenomena.

Several investigators have studied the flow and heat-transfer characteristics for configurations similar to that described above. Erdogan [1, 2] investigated the temperature distribution for fluid contained between two concentric spheres. The outer sphere rotated at a given rate while the inner was stationary. Secondary flows were ignored as the velocity field was found from Stokes' equation. Results for the temperature distribution were presented for various thermal boundary conditions. A

similar study by Avudainayagam [3] found that the overall rate of heat transfer from a rotating inner sphere to a stationary outer sphere was unaffected by convection. This is not unexpected since the Stokes' flow approximation was used for the velocity distribution.

Singh [4] and Bentwich [5] have studied the heat-transfer characteristics for a rotating sphere immersed in an infinite fluid medium. Singh considered the inner sphere to be at a constant temperature and the temperature of the fluid far from the rotating sphere was assumed uniform. Viscous dissipation was included. Isotherms were found to be surfaces of revolution which were closer to the spherical surface at the North Pole than at the Equator. Bentwich used a perturbation solution method for small Péclét and Reynolds numbers to find the temperature distribution for both the solid, rotating sphere and the surrounding fluid. A constant strength heat source was assumed at the center of the sphere. Solutions were presented as functions of the ratio of the conductivities of the sphere and fluid. Isotherms were of the same general shape as those reported by Singh.

Experimental results for the heat transfer of a rotating sphere to or from an infinite fluid medium have been reported by Nordlie and Kreith [6] and Kreith, *et al.* [7]. Data were presented for wide ranges of Reynolds, Grashof, and Prandtl numbers. Pedlosky [8] presented a linearized solution for stratified fluid contained between two concentric, differentially rotating spheres of narrow gap. It was found that the radial stratification had a significant effect on the flow field. The flow field in a rotating, heated spherical annulus for arbitrary radius ratios was studied analytically by Riley [9] and Riley and Mack [10]. The gravitational field was assumed to be uniform and parallel to the rotation axis. A perturbation solution method was used and results were presented for small Reynolds numbers (of order 1). It was shown that secondary flows as well as contours of constant temperature were strongly dependent on the ratio Gr/Re^2. Experimental data for a geometry similar to that of Riley and Mack were presented by Askin [11] and Maples, *et al.* [12].

The present work extends that of previous investigators by allowing solutions to be found to the coupled Navier–Stokes and energy equations for flow parameters much larger than permitted by perturbation methods and by considering combined modes of heat transfer. Here, the fluid is assumed to be unstably stratified with the gravitational field acting in the radial direction. The solutions are seen to be a complicated function of buoyancy and rotational effects as well as the geometry.

2. ANALYSIS

The system of equations describing the flow field for this combined convection situation is quite similar to that given in Part 1 (equations 1–3) for forced convection. The dependent and independent variables used here to describe the flow field are identical to those in Part 1. However, the flow geometry (Fig. 1, Part 1) is now in a uniform radial gravitational acceleration field placed at the center of the spheres. Thus, $\mathbf{g} = -g_0\mathbf{e}_r$ where g_0 is constant. The introduction of a gravitational field combined with a Boussinesq fluid [13] requires the addition of a body force term to the governing momentum equation [equation (2), Part 1]. This term has the effect of completely coupling the momentum and energy equations, as follows [14]:

$$\frac{1}{Re}\tilde{D}^2\Omega = \frac{1}{r^2\sin\theta}\frac{\partial(\Omega,\psi)}{\partial(r,\theta)}, \tag{1}$$

$$\frac{1}{Re}\tilde{D}^4\psi = -\frac{Gr}{Re^2}\sin\theta\frac{\partial\zeta}{\partial\theta} + \frac{1}{r^2\sin\theta}\left\{\frac{2}{r\sin\theta}\times\left[\Omega\frac{\partial(-r\sin\theta,\Omega)}{\partial(r,\theta)} + \tilde{D}^2\psi\frac{\partial(-r\sin\theta,\psi)}{\partial(r,\theta)}\right] + \frac{\partial(\tilde{D}^2\psi,\psi)}{\partial(r,\theta)}\right\}, \tag{2}$$

and

$$\frac{1}{Re}\nabla^2\zeta = \frac{Pr}{r^2\sin\theta}\frac{\partial(\zeta,\psi)}{\partial(r,\theta)} \tag{3}$$

where the Jacobian notation has been used.

The boundary conditions are the same as in Part 1: the fluid velocity and temperature at a surface equals the respective surface velocity and temperature.

As in the forced convection case, the governing equations for these combined convection flows are written in dimensionless form using the same characteristic time, length, and temperature references. Again, dimensionless parameters evolve including η, $\tilde{\mu}$, Re, and Pr as before. The remaining dimensionless parameter is the Grashof number $Gr = g_0\beta(T_2 - T_1)R_2^3/\nu^2$ which appears in equation (2). If the inner sphere is warmer than the outer sphere, $T_1 > T_2$ and Gr is negative. This situation may be thermally unstable, and in the absence of rotation is analogous to the Bénard problem. When the spheres are rotating at different rates, heating either sphere modifies the basic shear driven secondary flow. The extent of this modification is a complicated function of all the parameters of the problem.

It proves convenient in convection calculations to consider fixed values of the ratio Gr/Re^2. The forced convection problem is given by $Gr/Re^2 = 0$, thereby uncoupling equations (2) and (3). Here we consider the values $Gr/Re^2 < 0$, corresponding to the combined convection problem. Solutions are obtained to this fully coupled problem using the same techniques described in Part 1.

Since this is a parametric study, values of Gr/Re^2 were chosen to illustrate trends. In some cases, the Grashof numbers become quite large and may

perhaps lead to supercritical values of the Rayleigh number ($Ra = GrPr$). However, the authors are not acquainted with any existing research into the thermal stability of a fluid in a differentially rotating spherical annulus. The stability of the results presented here is, then, still open for further discussion.

3. DISCUSSION OF THE RESULTS

Calculations were made for $\tilde{\mu} = 0$, ∞, and $-1/3$, representing three widely different flow configurations. The value $\tilde{\mu} = 0$ corresponds to a rotating inner sphere with the outer sphere at rest, while the case $\tilde{\mu} = \infty$ is a rotating outer sphere with a fixed inner sphere. When $\tilde{\mu} = -1/3$ both spheres are rotating with $\omega_1 = -3\omega_2$. In order to limit the number of calculations, we take $Pr = 1$ and $\eta = 0.5$. A more extensive range of parameters is discussed in Douglass [14], and results for stable stratification are given by Shaughnessy and Douglass [15]. For each of the above configurations, various values of Gr/Re^2 (corresponding to the relative significance of buoyancy forces) were considered.

Figures 1–5 show the flow which occurs for $Re = 100$ and $\tilde{\mu} = -1/3$. In Fig. 1, secondary flow streamlines in the upper portion of a meridian plane show the effects of increasing thermal stratification. The shear driven secondary flow of Fig. 1(a) ($Gr/Re^2 = 0$) consists of two counter rotating toroidal eddies. The eddy near the inner sphere has a strong counterclockwise circulation; the other eddy has a slightly weaker clockwise circulation. The differences in the strength and direction of the flow in these convective motions reflect the fact that the inner sphere is rotating three times as fast as the outer sphere, and in the opposite direction.

For $Gr/Re^2 = -1$, the buoyancy and centrifugal forces are of the same order of magnitude. Figure 1(b) shows that the clockwise eddy located near the outer sphere now occupies a wider portion of the annulus near the North Pole (i.e. $\theta \simeq 0$). The counterclockwise eddy has grown slightly in strength, but is otherwise unchanged. As Gr/Re^2 increases through negative values, the secondary flow continues to be distorted. The eddies migrate, reducing the amount of contact between them. A current formed at the interface of the two eddies which initially flowed northward and was parallel to the rotating surfaces for $Gr/Re^2 = 0$, gradually steepens until it becomes nearly perpendicular to the rotation axis and tangent to the inner surface. For $Gr/Re^2 = -3$, the counterclockwise eddy occupies all of the annulus in the equatorial region, while the clockwise eddy dominates the northern latitudes. The circulation of both eddies has increased in the process.

These phenomena can be explained in terms of the centrifugal and buoyancy forces acting on fluid elements. Consider the case for which buoyancy forces are vanishingly small, i.e. forced convection. The basic secondary flow is driven by the unbalanced centrifugal force field established by the

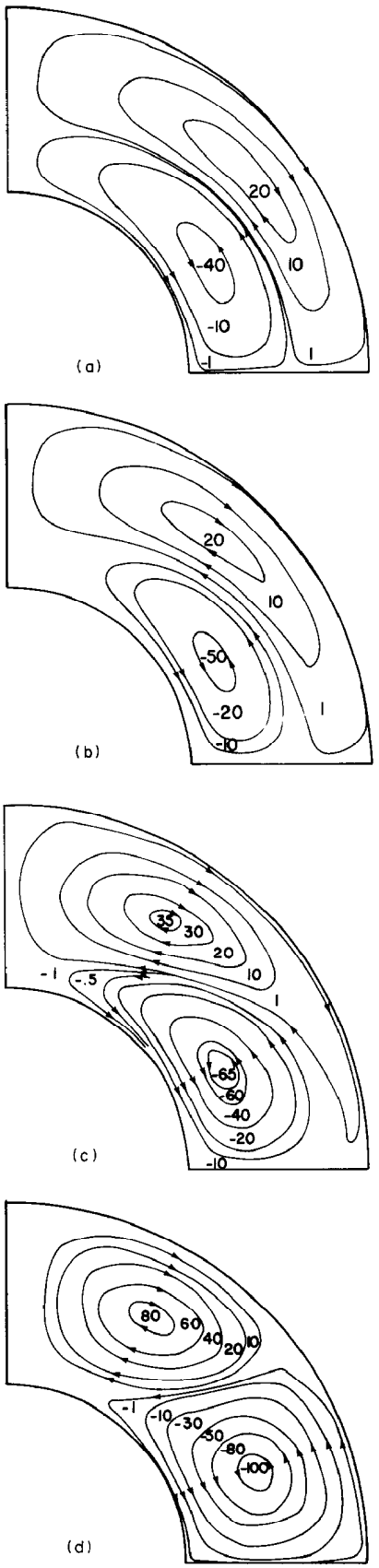

FIG. 1. Secondary flows ($10^4\psi$) for $Re = 100 = \omega_2 R_2^2/\nu$, $Pr = 1$, $\eta = 0.5$, and $\tilde{\mu} = -1/3$: (a) $Gr/Re^2 = 0$; (b) $Gr/Re^2 = -1$; (c) $Gr/Re^2 = -2$; (d) $Gr/Re^2 = -3$.

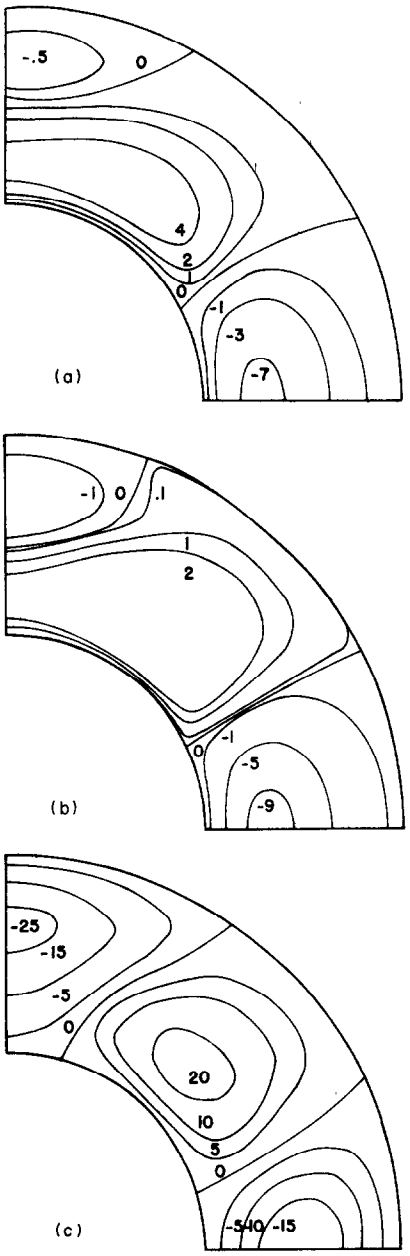

FIG. 2. $10^2(\zeta - \zeta_c)$ for $Re = 100 = \omega_2 R_2^2/\nu$, $Pr = 1$, $\eta = 0.5$, and $\tilde{\mu} = -1/3$: (a) $Gr/Re^2 = 0$; (b) $Gr/Re^2 = -1$; (c) $Gr/Re^2 = -3$.

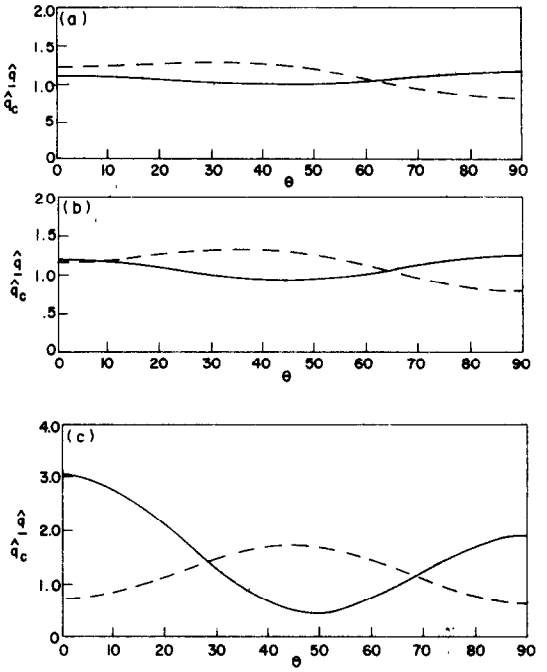

FIG. 3. Local heat flux for $Re = 100 = \omega_2 R_2^2/\nu$, $Pr = 1$, $\eta = 0.5$, and $\tilde{\mu} = -1/3$: (a) $Gr/Re^2 = 0$; (b) $Gr/Re^2 = -1$; (c) $Gr/Re^2 = -3$. (----) $r = \eta$, (——) $r = 1$.

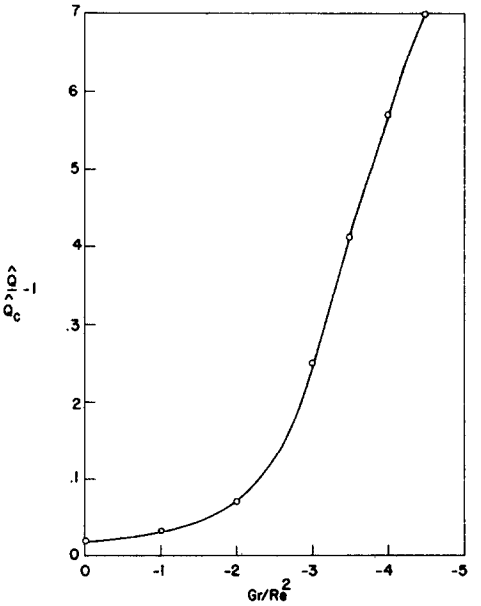

FIG. 4. The effect of increasing the buoyancy forces on the total heat flux. $Re = 100 = \omega_2 R_2^2/\nu$, $Pr = 1$, $\eta = 0.5$, and $\tilde{\mu} = -1/3$.

differential rotation of the two spheres. As fluid moves along the inner sphere from north to south, it is warmed by conduction heat transfer from the inner sphere. At the equator the warm fluid leaves the inner sphere and is carried northward on the current between the two eddies. As it returns to the starting point, the fluid is cooled by conduction heat transfer to the cooler fluid above it. A similar process occurs in the clockwise eddy.

With buoyancy forces present, the secondary flow is distorted by the tendency for warm fluid to rise and cool fluid to sink. This mechanism both strengthens and distorts the basic secondary flow. Figure 1(b) shows that the buoyancy forces on the cool fluid in the outer eddy overcome the centrifugal forces in the northern latitudes, causing a slight settling of the eddy boundary. Near the equator, however, the strong centrifugal forces prevent any upward motion of warm fluid. As the buoyancy forces grow stronger (Fig. 1c,d), they eventually dominate the centrifugal forces. The cooler fluid sinks, and the warm fluid rises. Since the buoyancy forces and the direction of motion generally coincide, the circulation in each eddy is enhanced.

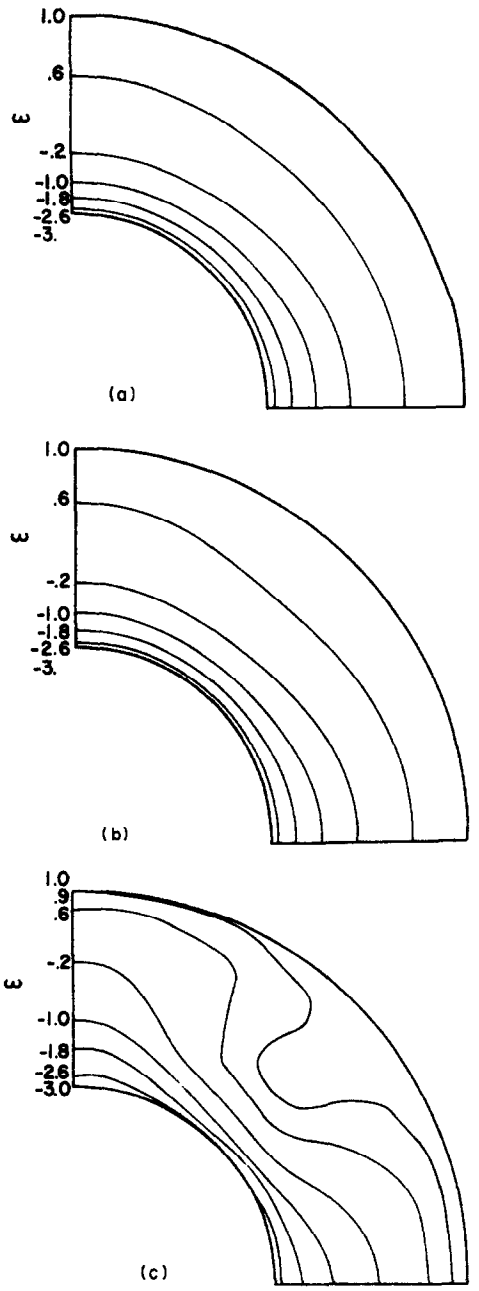

FIG. 5. Angular velocity contours for $Re = 100 = \omega_2 R_2^2/\nu$, $Pr = 1$, $\eta = 0.5$, and $\tilde{\mu} = -1/3$: (a) $Gr/Re^2 = 0$; (b) $Gr/Re^2 = -1$; (c) $Gr/Re^2 = -3$.

Figure 2 illustrates the effect of increasing buoyancy forces on the temperature distribution in the annulus. In order to show the effects of convection, lines of constant $\zeta - \zeta_c$ have been plotted. $\zeta_c(r)$ is the conduction temperature distribution given by

$$\zeta_c(r) = (1-\eta/r)/(1-\eta). \tag{4}$$

The deviation $\zeta - \zeta_c$ is therefore a sensitive measure of the effects of convection. When the Grashof number is negative, as it is here, regions containing fluid which is warmer than the conduction temperature have negative $\zeta - \zeta_c$ values.

In the case of forced convection, regions of relatively warm fluid are found near the equator and near the North Pole (Fig. 2a). The concentration of warm fluid at the equator spans the annulus, while at the pole, the warm fluid is confined to the outer half of the gap. A large region of relatively cool fluid occupies the mid-latitudes. As the magnitude of Gr/Re^2 increases, the northern concentration of warm fluid increases in width until it spans the annulus. Figure 2(c) shows the $\zeta - \zeta_c$ contours occurring for $Gr/Re^2 = -3$. A comparison of Figs. 1 and 2 indicates that the distorted secondary flows are responsible for these temperature distribution effects.

Additional insight into the effects of convective activity on the heat transfer in the annulus can be gained from the surface heat flux profile $\hat{q}(\theta)$. Figure 3 shows the latitudinal profile of $\hat{q}/\hat{q}_c$, where $\hat{q}_c$ is the conduction heat flux. The ratio is given by either equations (10) or (14) of Part 1. Figures 3(a) and (b) show that for forced convection, and flows with relatively small buoyancy forces, there is little enhancement of the local heat flux. The secondary flows are relatively ineffectual in convecting cool fluid to the hot surface, and vice-versa, because both surfaces are separated by the secondary swirl. Once the eddies begin to span the gap, however, the heat transfer is greatly enhanced as shown in Fig. 3(c) (cf. Fig. 1). The central fluid current is especially effective in bringing cool fluid in contact with the hot inner sphere. On the outer sphere, the updrafts at the equator and North Pole bring warm fluid into contact with the cool surface resulting in large local heat fluxes.

The total heat flux, $\hat{Q}$, normalized by the conduction flux, $\hat{Q}_c$, is found by integrating the local flux ratio, weighted by $\sin\theta$ (because of surface area effects), over the surface of spheres. The total conduction heat flux is found to be

$$\frac{\hat{Q}_c}{R_2\kappa(T_2-T_1)} = \frac{4\pi\eta}{(1-\eta)}; \tag{5}$$

the same value for each spherical surface. $\hat{Q}/Q_c$ is given by either equation (11) or (15) of Part 1. The total heat flux is shown in Fig. 4. The rapid increase in $\hat{Q}/Q_c$ for increasing buoyancy forces reflects the marked changes in the secondary flows as the buoyancy forces become strong. Increasing the Reynolds number also enhances the total heat transfer. This trend is shown in Table 1 for $Gr/Re^2 = -1$. The effect, however, is not as dramatic for the Reynolds numbers listed as it is for increasing the buoyancy forces.

Table 1. The total heat flux for $Gr/Re^2 = -1$, $Pr = 1$, $\eta = 0.5$, and $\tilde{\mu} = -1/3$

$Re = \omega_2 R_2^2/\nu$	$\hat{Q}/\hat{Q}_c - 1$
10	3.7×10^{-6}
100	2.9×10^{-2}
125	6.7×10^{-2}
150	1.3×10^{-1}
175	2.0×10^{-1}

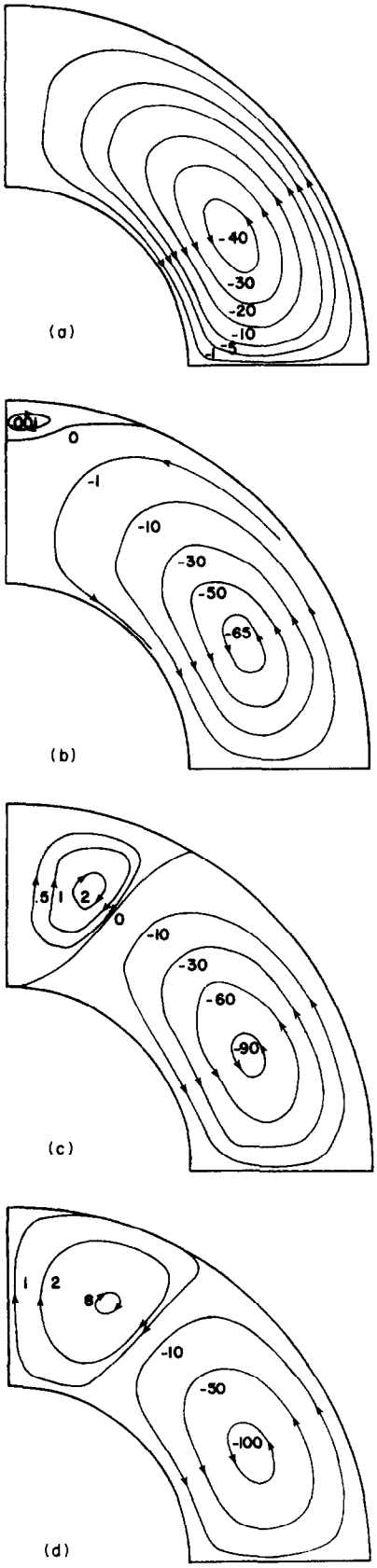

FIG. 6. Secondary flows ($10^4\psi$) for $Re = 200 = \omega_1 R_2^2/\nu$, $Pr = 1$, $\eta = 0.5$, and $\tilde{\mu} = 0$: (a) $Gr/Re^2 = 0$; (b) $Gr/Re^2 = -0.25$; (c) $Gr/Re^2 = -0.4$; (d) $Gr/Re^2 = -0.5$.

Contours of constant values of the (dependent) angular velocity variable, ω, are shown in Fig. 5. In each illustration, the curves are surfaces of revolution. For forced convection, they are nearly spherical in nature, but as the buoyancy forces increase, the contours become quite distorted. This distortion is associated with the secondary flow which transports the "slower" fluid to the middle latitudes [cf. Fig. 1(d)].

The second series of results is for $Re = 200$ and $\tilde{\mu} = 0$, i.e. the outer sphere is at rest. Results shown are limited to values of Gr/Re^2 between 0 and 0.5. Figure 6 shows how the secondary flow changes in response to increasing buoyancy forces. The forced convection flow consists of a single toroidal eddy driven by shear forces at the inner boundary. Upon heating the inner sphere, buoyancy forces begin to influence the secondary flow near the North Pole, where the centrifugal forces are weakest. A weak clockwise circulation is established which gains strength as the buoyancy forces become stronger. At $Gr/Re^2 = -0.5$, this northern eddy completely spans the gap but its circulation remains weak in comparison to the counterclockwise equatorial eddy.

The plots of $\zeta - \zeta_c$ for this series of flows with small buoyancy forces have a different character from that seen for $\tilde{\mu} = -1/3$, but as buoyancy forces become more important their character is quite similar. Figure 7 shows that for $Gr/Re^2 = 0$, a region

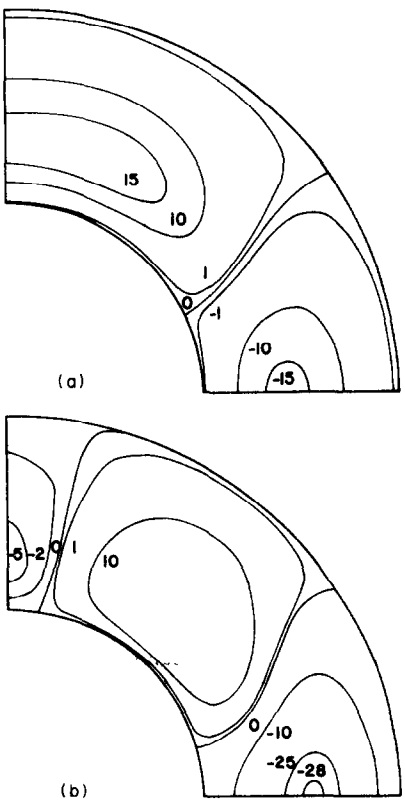

FIG. 7. $10^2(\zeta - \zeta_c)$ for $Re = 200 = \omega_1 R_2^2/\nu$, $Pr = 1$, $\eta = 0.5$, and $\tilde{\mu} = 0$: (a) $Gr/Re^2 = 0$; (b) $Gr/Re^2 = -0.5$.

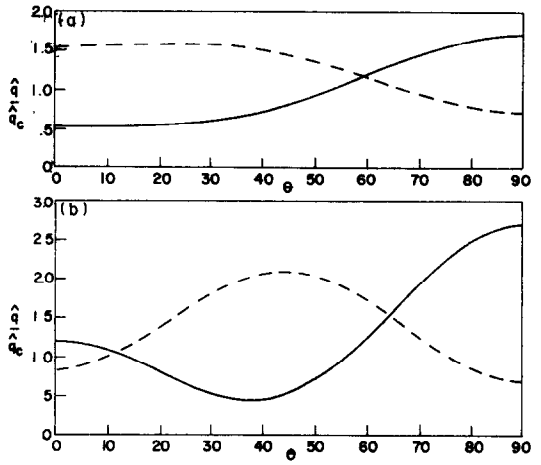

FIG. 8. Local heat flux for $Re = 200 = \omega_1 R_2^2/\nu$, $Pr = 1$, $\eta = 0.5$, and $\tilde{\mu} = 0$: (a) $Gr/Re^2 = 0$; (b) $Gr/Re^2 = -0.5$. (----) $r = \eta$, (——) $r = 1$.

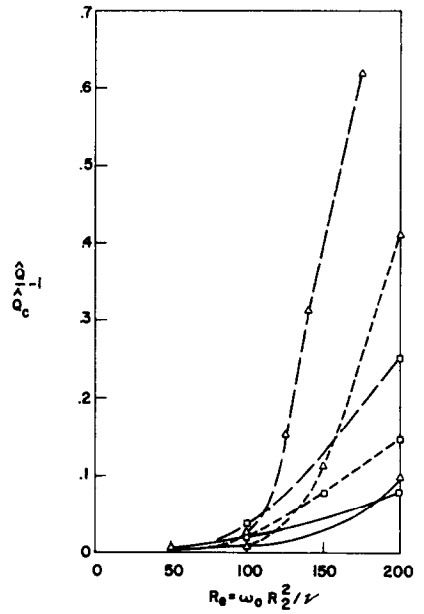

FIG. 9. The effect of increasing the Reynolds number on the total heat flux for $Pr = 1$, $\eta = 0.5$, and for $\tilde{\mu} = 0$ ($\triangle$) and $\mu = \infty$ ($\square$). (——) $Gr/Re^2 = 0$, (----) $Gr/Re^2 = -0.5$, and (– – –) $Gr/Re^2 = -1$.

of relatively hot fluid occurs near the equator, with cool fluid in the northern latitudes. These concentrations are the result of updrafts and downdrafts in the secondary flow field. The single toroidal eddy of Fig. 6 for $Gr/Re^2 = 0$ ultimately is replaced by two counter-rotating eddies at $Gr/Re^2 = -0.5$. These eddies contribute two updrafts and one downdraft, consequently, the $\zeta - \zeta_c$ plot of Fig. 7(b) shows two hot regions and one cool region.

Figure 8 shows that the local heat flux results for $\tilde{\mu} = 0$ are also qualitatively similar to those for $\tilde{\mu} = -1/3$ when two eddies occur in each flow and span the gap. Otherwise, the heat flux results reflect the differences in convection associated with a single eddy (Fig. 6a) and two, layered eddies (Fig. 1a). The variation of the total heat flux with Reynolds number for $\tilde{\mu} = 0$ is shown in Fig. 9 for forced

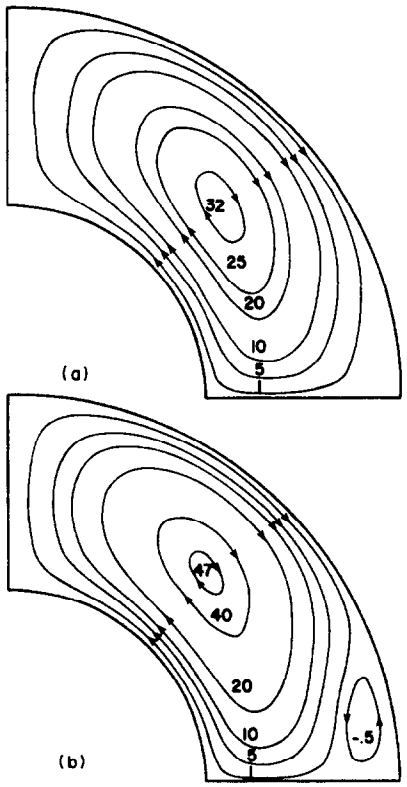

FIG. 10. Secondary flows ($10^4\psi$) for $Re = 200 = \omega_2 R_2^2/\nu$, $Pr = 1$, $\eta = 0.5$, and $\tilde{\mu} = \infty$: (a) $Gr/Re^2 = 0$; (b) $Gr/Re^2 = -0.5$.

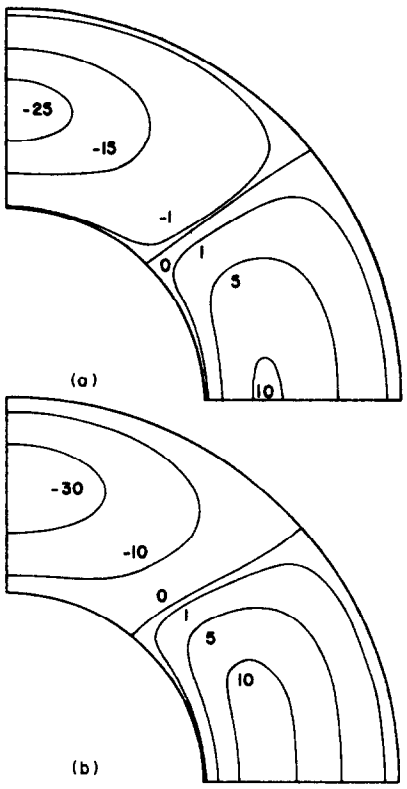

FIG. 11. $10^2(\zeta - \zeta_c)$ for $Re = 200 = \omega_2 R_2^2/\nu$, $Pr = 1$, $\eta = 0.5$, and $\tilde{\mu} = \infty$: (a) $Gr/Re^2 = 0$; (b) $Gr/Re^2 = -0.5$.

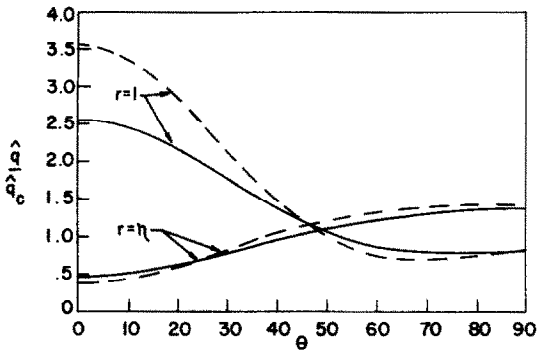

FIG. 12. Local heat flux for $Re = 200 = \omega_2 R_2^2/\nu$, $Pr = 1$, $\eta = 0.5$, $\tilde{\mu} = \infty$, $Gr/Re^2 = 0$ (——) and $Gr/Re^2 = -0.5$ (----).

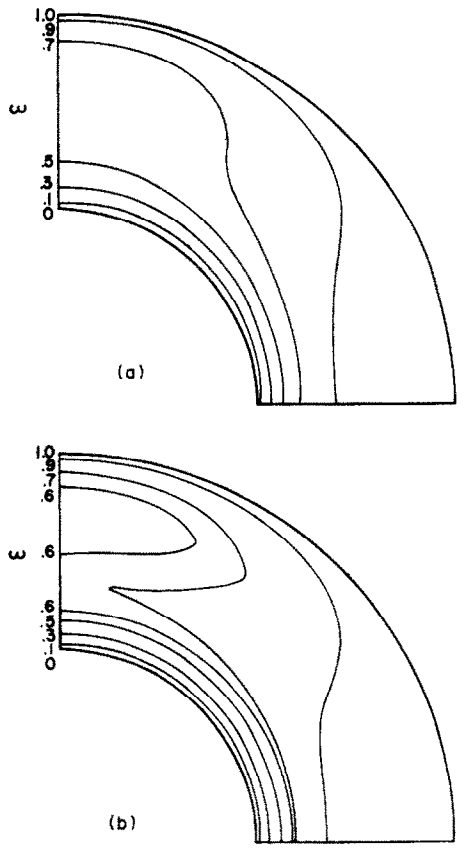

FIG. 13. Angular velocity contours for $Re = 200 = \omega_2 R_2^2/\nu$, $Pr = 1$, $\eta = 0.5$, and $\tilde{\mu} = \infty$: (a) $Gr/Re^2 = 0$; (b) $Gr/Re^2 = -0.5$.

convection as well as combined convection. It is shown that, as for $\tilde{\mu} = -1/3$, increasing the buoyancy forces has a much larger effect than does increasing the Reynolds number.

The final series of results, shown in Figs. 10–13, share many features with the flows just described. In this series of flows, the inner sphere is fixed while the outer sphere rotates ($\tilde{\mu} = \infty$). For $Gr/Re^2 = 0$, the secondary flow consists of a single eddy with clockwise circulation. Buoyancy forces first distort the secondary flow near the equator and eventually a small counterclockwise motion is established there (Fig. 10). At $Gr/Re^2 = -0.5$, a well defined weak eddy appears near the outer sphere in the equatorial region. This eddy does not span the gap, which, as seen earlier, has important consequences for the temperature distributions. The $\zeta - \zeta_c$ contours of Fig. 11 show that the counterclockwise eddy has far less effect on the temperature field than in earlier double eddy flows. This is a result of both its weakness and the fact that the eddy remains confined to a region near the outer sphere only. The local heat flux results (Fig. 12) in particular are quite different than in cases where the convective eddies span the annulus.

Since there is only one large eddy which spans the annulus, the results for increased buoyancy forces are quite similar to those for forced convection. The differences in the results are caused more by the enhancement of the circulation of the clockwise eddy than by buoyant distortion. This increase in secondary flow is caused by the buoyant effect of the hot fluid near the polar region. This buoyant force increases the magnitude of the secondary flow swirl because it tends to drive the fluid in the direction it is already going. The total heat flux results for this series of flows are shown in Fig. 9. As expected, the heat flux increases as both Re and Gr/Re^2 increase, though more strongly with the latter. The angular velocity contours are shown in Fig. 13 and reflect a relatively small change in shape for increased buoyancy forces. This is expected since the secondary flow is relatively unchanged.

4. STRATIFICATION AND TORQUE

The torque required to rotate a sphere, $\hat{M}$, was found by integrating the shear stress over the surface of the sphere to obtain

$$\hat{M} = 4\pi\mu r^4 \int_{\theta=0}^{\pi/2} \sin^2\theta \frac{\partial}{\partial \hat{r}}\left(\frac{\hat{V}_\phi}{\hat{r}}\right) d\theta. \qquad (6)$$

It is useful to non-dimensionalize the torque by its value for creeping flow, $\hat{M}_0$. This low Reynolds number torque is given by $\hat{M}_0 = 8\pi\mu R_1^3(\omega_1 - \omega_2)/(1 - \eta^3)$. In this case, the secondary flows become unimportant, and the flow field is described entirely by the primary flow [$\omega(r,\theta)$ and $\rho_c(r,\theta)$].

Typical results are shown in Fig. 14. To limit the number of results presented, only data for $\eta = 0.5$ and $Pr = 1.0$ are shown. Other cases may be found in [14]. Figure 14 summarizes the torque dependence on both Re and Gr/Re^2 for different angular velocity ratios including a stationary outer sphere ($\tilde{\mu} = 0$), a stationary inner sphere ($\tilde{\mu} = \infty$), and a contrarotating sphere ($\tilde{\mu} = -1/3$). In each case the forced convection (or isothermal flow) results are presented for comparison. These include theoretical results from Munson [16] and the experimental results from Waked [17].

In all cases, the torque is seen to be an increasing function of both Re and Gr/Re^2. This is not unexpected since an increase in either of these parameters increases the magnitude of the secondary flow circulation. Not only does the magnitude of the secondary flow vary with these parameters, but the

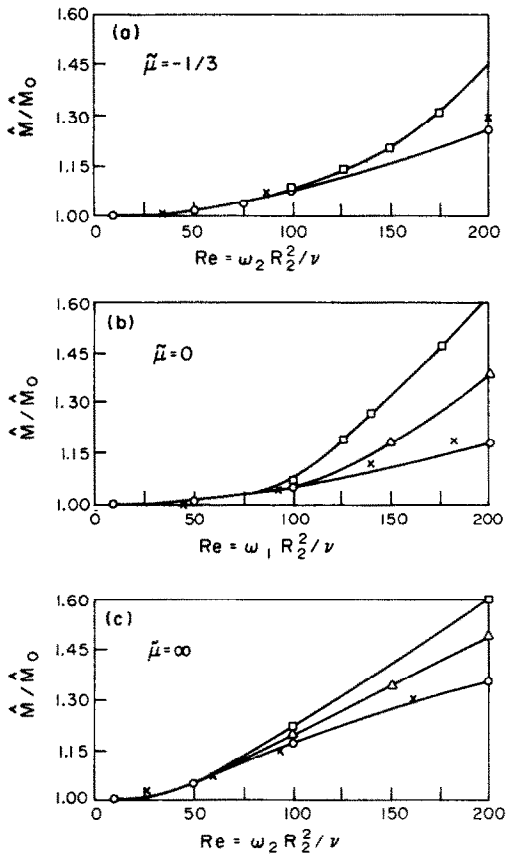

FIG. 14. The effect of stratification on the torque required to rotate the spheres. $Pr = 1$, $\eta = 0.5$, and (a) $\tilde{\mu} = -1/3$, (b) $\tilde{\mu} = 0$, and (c) $\tilde{\mu} = \infty$. $Gr/Re^2 = 0$ (○), $Gr/Re^2 = -0.5$ (△), and $Gr/Re^2 = -1$ (□). Experimental results for $Gr/Re^2 = 0$ and $\eta = 0.44$ [17] (×).

shape of the secondary flow swirls also changes. This is illustrated in Figs. 1, 6, and 10. Since the primary and secondary flows are coupled [cf. equations (1) and (2)], the enhanced secondary flow (given in terms of ψ) alters the primary flow (given in terms of Ω), resulting in increasing values of $\hat{M}/\hat{M}_0$. The primary flow can also be altered through the coupling of the energy and momentum equations through the body force term in the momentum equation [cf. equations (2) and (3)]. As shown, for example in Fig. 5, this effect may be quite dramatic. The net result is also an increased value of $\hat{M}/\hat{M}_0$ as the buoyancy forces (Gr/Re^2) are increased. In all cases investigated, the limiting isothermal, creeping flow case ($Gr/Re^2 \to 0$) gave the smallest torque. That is, $\hat{M}/\hat{M}_0 > 1$ except for the special case of $\hat{M} = \hat{M}_0$ when $Re = 0$.

5. CONCLUSION

The interaction of buoyancy forces with the shear-driven secondary flow in the annulus leads to many interesting fluid motions. For the moderate Reynolds numbers studied here, a common configuration for the secondary flow is a pair of counter-rotating eddies. The location of these eddies, their size, strength, and direction of flow are functions of the angular velocity ratio $\tilde{\mu}$, and Gr/Re^2. The latter parameter is a measure of the relative strengths of buoyancy forces as compared with centrifugal forces.

As expected, the temperature distributions, local heat flux, and torque are strongly dependent on the secondary flow configuration. Strong jet-like fluid motions along the line of contact between eddies produce large distortions of the otherwise nearly spherical isotherms and angular velocity contours. The local heat flux on the surface is highly correlated with updrafts and downdrafts in the annulus. In this regard, eddies which make contact with both spherical surfaces (that is, those that span the annulus) are far more effective in transferring heat than those confined near one surface. Likewise, two eddies appear more effective than one, provided both span the annulus. The total rate of heat transfer and torque increase as both Re and Gr/Re^2 increase, though more strongly with the latter parameter.

A more extensive presentation of results for this geometry may be found in [14].

Acknowledgement—The support of NSF Grant ENG7518398, the Engineering Research Institute, Iowa State University, and the Engineering Research Center, University of Nebraska-Lincoln for portions of this work has been appreciated.

REFERENCES

1. M. Erdogan, Heat transfer in an incompressible viscous fluid between two concentric rotating spheres, *Bull. Istanbul Tech. Univ.* **17**, 77–86 (1964).
2. M. Erdogan, Transmission de la chaleur á un fluide visqueux se mouvant entre deux spheres concentriques tournantes, *Z. Angew. Math. Phys.* **15**, 66–67 (1964).
3. A. Avudainayagam, Heat transfer from a slowly rotating sphere, *Appl. Scient. Res.* **26**, 18–22 (1972).
4. S. Singh, Heat transfer by laminar flow from a rotating sphere, *Appl. Scient. Res.* **9**, 197–205 (1960).
5. M. Bentwich, The temperature distribution inside a rotating sphere and in the entire flow field around it, *Israel J. Technol.* **9**, 1–6 (1971).
6. R. Nordlie and F. Kreith, Convective heat transfer from a rotating sphere, in *International Developments in Heat Transfer (Proceedings of the* 1961–62 *Heat Transfer Conference)*, pp. 461–467 (1962).
7. F. Kreith, L. Roberts, J. Sullivan and S. Sinha, Convection heat transfer and flow phenomena of rotating spheres, *Int. J. Heat Mass Transfer* **6**, 881–895 (1963).
8. J. Pedlosky, Axially symmetric motion of a stratified, rotating fluid in a spherical annulus of narrow gap, *J. Fluid Mech.* **36**, 401–415 (1969).
9. T. Riley, Thermal influence on the slow viscous flow of a fluid between rotating concentric spheres, PhD Dissertation, University of Texas, Austin, Texas (1971).
10. T. Riley and L. Mack, Thermal effects on slow viscous flow between rotating concentric spheres, *Int. J. Nonlinear Mech.* **7**, 275–288 (1972).
11. K. Askin, Convective heat transfer from a rotating inner sphere to a stationary outer sphere, MS Thesis, Auburn University, Auburn, Alabama (1971).
12. G. Maples, D. Dyer, K. Askin and D. Maples, Convective heat transfer from a rotating inner sphere to a stationary outer sphere, *J. Heat Transfer* **95**, 546–547 (1973).
13. D. Gray and A. Giorgini, The validity of the Boussinesq approximation for gases and liquids, *Int. J. Heat Mass Transfer* **19**, 545–551 (1976).

14. R. Douglass, Combined natural and forced thermal convection in a rotating spherical annulus PhD Dissertation, Duke University, Durham, N.C (1975).
15. E. Shaughnessy and R. Douglass, The effect of stable stratification on the motion in a rotating spherical annulus, *Int. J. Heat Mass Transfer* **21**, 1251–1259 (1978).
16 B. Munson, Hydrodynamic stability of flow between rotating spheres and rotating-sliding cylinders, PhD Dissertation, University of Minnesota, Minneapolis, MN (1970).
17 A M Waked, Experimental investigation of flow between rotating spheres, PhD Dissertation, Iowa State University, Ames, IA (1977).

CONVECTION THERMIQUE DANS DES ESPACES ANNULAIRES SPHERIQUES—I CONVECTION FORCEE

Résumé—On considère la convection forcée stationnaire d'un fluide visqueux entre deux sphères concentriques, maintenues à des températures différentes et tournant autour d'un axe commun avec des vitesses angulaires différentes. On résout de façon approchée les équations par une solution de perturbation régulière valable pour les faibles nombres de Reynolds et par une solution de Galerkin modifiée pour les nombres de Reynolds modérés. On présente les configurations d'écoulement, de distribution de température et les caractéristiques du transfert thermique pour les différents cas considérés. Les résultats théoriques sur le transfert thermique pour des nombres de Reynolds petits ou modérés avec la sphère extérieure fixe sont comparés à des résultats expérimentaux antérieurs et relatifs à des grands nombres de Reynolds. On montre la différence entre la conduction, l'écoulement de Stokes et la convection de couche limite.

THERMISCHE KONVEKTION IN ROTIERENDEN, KUGELFÖRMIGEN RINGRÄUMEN—II—GESCHICHTETE STRÖMUNGEN

Zusammenfassung—Für ein zähes "Boussinesq-Fluid", das sich zwischen 2 konzentrischen Kugeln befindet, wird stationäre gemischte thermische Konvektion betrachtet. Die Kugeln werden auf unterschiedlichen Temperaturen gehalten und rotieren mit unterschiedlicher Winkelgeschwindigkeit um eine gemeinsame Achse. Ein gleichmäßiges radiales Beschleunigungsfeld wirkt auf das Fluid ein. Mittels einer modifizierten Galerkin-Methode erhält man Näherungslösungen der maßgeblichen Gleichungen im Bereich mäßiger Reynolds-Zahlen. Als Ergebnis werden die Stromlinienbilder, die Temperaturverteilungen und das Verhalten von Wärmeübergang und Drehmoment dargestellt, und zwar für verschiedene Winkelgeschwindigkeitsverhältnisse und Schichtungsgrade. Es wird gezeigt, daß sich bei zunehmenden Auftriebskräften das Bild der Primär- und Sekundärströmung ebenso ändert wie die Temperaturverteilung. Der Gesamtbetrag von Wärmeübergang und Drehmoment nimmt dabei zu.

ТЕПЛОВАЯ КОНВЕКЦИЯ В ЗАЗОРЕ МЕЖДУ ВРАЩАЮЩИМИСЯ СФЕРАМИ. ЧАСТЬ 2. СТРАТИФИЦИРОВАННОЕ ТЕЧЕНИЕ

Аннотация — Рассматривается стационарная смешанная теплова конвекция вязкой жидкости в зазоре между двумя концентрическими сферами в приближении Буссинеска. Сферы находятся при различных температурах и вращаются с различными угловыми скоростями вокруг общей оси. Жидкость подвергается воздействию однородного радиального гравитационного поля. С помощью модифицированного метода Галеркина получены приближенные решения исходных уравнений для средних значений числа Рейнольдса Для нескольких отношений угловых скоростей и степеней стратификации течения приводятся картина течения, распределение температур, а также характеристики теплообмена и крутящий момент. Показано, что с увеличением подъёмной силы происходит изменение первичной и вторичной картин течения, а также распределения температур В результате возрастают суммарная интенсивность теплообмена и крутящий момент.